An unconditionally energy-stable second-order time-accurate numerical scheme for the coupled Cahn–Hilliard system in copolymer/homopolymer mixtures

Yibao Li [a], Lujing Zhang [a], Qing Xia [a], Qian Yu [a], Junseok Kim [b],*

[a] School of Mathematics and Statistics, Xi'an Jiaotong University, Xi'an 710049, China
[b] Department of Mathematics, Korea University, Seoul 02841, Republic of Korea

A B S T R A C T

In this article, we present an unconditional energy stable numerical method for the coupled Cahn–Hilliard system for homopolymer and copolymer mixtures in two- and three-dimensional spaces. By combining a Crank–Nicolson-type method with a nonlinearly stabilized splitting method, a second-order accurate numerical scheme is constructed. To efficiently solve the discrete system, we use a fast iterative Fourier transform method. We prove the unconditional energy stability of the proposed method. Therefore, a large time step can be adopted. Various numerical experiments are performed to prove the performance of the proposed scheme.

1. Introduction

The intramolecular and intermolecular interactions within copolymers and homopolymers induce self-assembly into various ordered microstructures, including spheres, cylinders, bicontinuous structures, and hierarchical structures [1–6]. The shape effect in blends plays an important role in the improvement of physical properties, which have obtained expensive attention in various fields, for example, enhancing the chemical performance in chemical industry, biomedical research, and electrical applications [7–10].

Many polymer patterns can undergo self-assembly into various morphologies to minimize their free energy functional [11–14]. Phase-field theory, obtained by a sequence of approximations from dynamical density functional theory [15], is an efficient modeling framework to study the numerical simulation of phase evolution and the interface transition [16–21]. Instead of defining the regions of different components, only an evolution equation needs to be solved under the phase field framework [22]. Leibler [23] proposed a phase field functional with a long-range term, which was crucial for the microphase separation. However, their method only could be applied for weak separation. Ohta and Kawasaki [24,25] put forward a free energy functional for the diblock copolymers and took the long-range and short-range interaction into account. Ohta and Ito [26] carried out the computer simulations of phase separation for the first time and investigated the dynamics and morphology of phase transition in diblock copolymer–homopolymer mixtures. Uneyama and Doi [27,28] derived an expression for the diblock copolymers' free energy. Their function was composed of the density distribution of the monomer of each block, which is a powerful generalization of Ohta–Kawasaki theory.

Up to now, various numerical methods have been proposed for phase field functional in copolymer mixtures [29–35]. Wu and Dzenis [36] adopted a semi-implicit Fourier-spectral algorithm to form lamellar nano-structures with potential applications in nanotechnology. Compared with the phase separation modeling for conventional coarse grained, the time steps selected were much larger. Glasner [37,38] studied the cross-sectional profile of a multilayered interface through a three-component phase-field equation. They established the basic structures and properties of copolymer multilayers. In [39], Cheng et al. adopted the invariant energy quadruplication method to transform the free energy into a quadratic form for the hydro-dynamically coupled phase field diblock copolymer equation. Furthermore, Zhao et al. [40, 41] reviewed the invariant energy quadratization strategy on discretizing phase-field models and techniques for solving diblock copolymer models. Gong et al. [42–44] introduced arbitrarily high order numerical algorithms for solving general phase-field models, which can be easily applied for the copolymer models.

Our goal of this paper is to propose a nonlinear numerical method for the coupled Cahn–Hilliard system employed in copolymer/homopolymer mixtures, which is unconditionally energy-stable and second-order accurate. By combining a Crank–Nicolson-type method

---

* Corresponding author.
  E-mail addresses: yibaoli@xjtu.edu.cn (Y. Li), cfdkim@korea.ac.kr (J. Kim).
  URLs: http://gr.xjtu.edu.cn/web/yibaoli (Y. Li), https://mathematicians.korea.ac.kr/cfdkim/ (J. Kim).

and a nonlinearly stabilized splitting method, a second-order time-accurate numerical scheme is constructed. The proof of unconditional energy stability will be given. To efficiently solve the discrete system, we will use a fast Fourier transform with an iterative method. A discrete energy-dissipation law for any large time step is proved to demonstrate the proposed method is stable. Some computational experiments are conducted to prove the proposed scheme's capabilities.

This research is organized as follows. In Section 2, we review the density functional model. In Section 3, we develop a second-order unconditional energy stable schemes and prove numerical stabilities. In Section 4, several numerical simulations are presented in two- and three-dimensions. Finally, some conclusions are presented in Section 5.

2. Model formulation

The copolymer/homopolymer mixtures can be considered as a mixture of two systems, which is driven by microphase separation and macrophase separation. The free energy functional's dissipation [25,26] models the process of the diblock copolymer melts:

$$\mathcal{E}(\phi, \psi) = \mathcal{E}_s(\phi, \psi) + \mathcal{E}_l(\phi, \psi). \tag{1}$$

The short-range energy $\mathcal{E}_s(\phi, \psi)$ is given by [45,46]

$$\mathcal{E}_s(\phi, \psi) = \int_{\Omega} \left(W(\phi, \psi) + \frac{\epsilon_\phi^2}{2} |\nabla \phi|^2 + \frac{\epsilon_\psi^2}{2} |\nabla \psi|^2 \right) d\mathbf{x}. \tag{2}$$

Here, ϕ describes the microphase separation between block A and B, ψ describes the macrophase separation between homopolymers and copolymers. The parameters ϵ_ϕ and ϵ_ψ increase with the thickness of components' propagating fronts. The function W has the form:

$$W(\phi, \psi) = \frac{1}{4}(\phi^2 - 1)^2 + \frac{1}{4}(\psi^2 - 1)^2 + a\phi\psi + b\phi^2\psi, \tag{3}$$

which ensures the values of ϕ and ψ fall within $[-1, 1]$. In addition, $\phi = 1$ represents the block A, $\phi = -1$ represents the block B [47], $\psi = -1$ corresponds to homopolymer rich domain, and $\psi = 1$ can be considered as a copolymer rich domain [48]. The function W has two coupling parameters a and b. The coupling parameter a leads to symmetry breaking between the microphase-separated domains and the coupling parameter b affects the short-range free energy $\mathcal{E}_s$ depending on the value of ψ [45]. The nonlocal energy is defined as

$$\mathcal{E}_l(\phi, \psi) = \frac{\sigma}{2} \int_{\Omega} \int_{\Omega} G(\mathbf{x} - \mathbf{y})(\phi(\mathbf{x}) - \bar{\phi})(\phi(\mathbf{y}) - \bar{\phi}) d\mathbf{y} d\mathbf{x}. \tag{4}$$

Here, σ is a positive phenomenological parameter, $\bar{\phi} = \int_{\Omega} \phi(\mathbf{x}) d\mathbf{x}/|\mathbf{\Omega}|$ is on behalf of the total mass. Specially, $\Delta G(\mathbf{x}, \mathbf{y})$ is defined $\Delta G(\mathbf{x}, \mathbf{y}) = -\delta(\mathbf{x}, \mathbf{y})$ and δ is Dirac delta function. Now by assuming $\varphi = (-\Delta)^{-1}(\phi - \bar{\phi})$, we can simplify Eq. (4) through the Green theorem [49,50]

$$\frac{\sigma}{2} \int_{\Omega} \int_{\Omega} G(\mathbf{x} - \mathbf{y})(\phi(\mathbf{x}) - \bar{\phi})(\phi(\mathbf{y}) - \bar{\phi}) d\mathbf{y} d\mathbf{x}$$

$$= \frac{\sigma}{2} \int_{\Omega} \Delta\varphi(\mathbf{x}) \left(\int_{\Omega} \Delta G(\mathbf{x} - \mathbf{y})\varphi(\mathbf{y}) d\mathbf{y} \right) d\mathbf{x} = \frac{\sigma}{2} \int_{\Omega} |\nabla\varphi|^2 d\mathbf{x}.$$

The energy functional $\mathcal{E}(\phi, \psi)$ in Eq. (1) can be rewritten as

$$\mathcal{E}(\phi, \psi) = \int_{\Omega} \left(W(\phi, \psi) + \frac{\epsilon_\phi^2}{2} |\nabla\phi|^2 + \frac{\epsilon_\psi^2}{2} |\nabla\psi|^2 + \frac{\sigma}{2} |\nabla\varphi|^2 \right) d\mathbf{x}. \tag{5}$$

The dynamic governing equations based on the gradients of the generalized chemical potentials, μ and ν can be defined as

$$\phi_t = M_\phi \Delta\mu, \tag{6}$$

$$\mu = W_\phi(\phi, \psi) - \epsilon_\phi^2 \Delta\phi - \sigma\varphi, \tag{7}$$

$$\psi_t = M_\psi \Delta\nu, \tag{8}$$

$$\nu = W_\psi(\phi, \psi) - \epsilon_\psi^2 \Delta\psi. \tag{9}$$

Here, the mobility tensor M_ϕ and M_ψ are diffusion rate and cross-diffusion rate, respectively. $W_\phi(\phi, \psi)$ and $W_\phi(\phi, \psi)$ are the first derivative of the function $W(\phi, \psi)$ in regard to ϕ and ψ, respectively. We use

the periodic boundary conditions for ϕ and ψ. This system satisfies the energy's laws of dissipation:

$$\frac{d\mathcal{E}}{dt} = \int_{\Omega} (\mu\phi_t + \nu\psi_t) d\mathbf{x} = \int_{\Omega} \left(M_\phi \mu \Delta\mu + M_\psi \nu \Delta\nu \right) d\mathbf{x}$$

$$= -\int_{\Omega} \left(M_\phi |\nabla\mu|^2 + M_\psi |\nabla\nu|^2 \right) d\mathbf{x} \leq 0, \tag{10}$$

which implies that the total energy functional $\mathcal{E}(\phi, \psi)$ decreases with time. Differentiating the total mass $\int_{\Omega} \phi(\mathbf{x}) d\mathbf{x}$ in regard to time, we have

$$\frac{d}{dt} \int_{\Omega} \phi(\mathbf{x}, \mathbf{t}) d\mathbf{x} = \mathbf{0} \tag{11}$$

which means that the total mass is conserved over time and $\bar{\phi} = \int_{\Omega} \phi(\mathbf{x}, 0) d\mathbf{x}/|\mathbf{\Omega}|$ is a constant.

3. Numerical scheme

In this Section, we introduce an unconditional energy-stable and second-order time-accurate scheme for Eqs. (6)–(9). We set the computational domain as $\Omega = [0, L] \times [0, L]$. The spatial step size is uniform as $h = L/N_x = L/N_y$, where N_x and N_y are even integers. The time step is $\Delta t = T/N_t$, where T is the finial time and N_t is the number of computational time steps. We denote $\phi_{ij}^n = \phi(x_i, y_j, n\Delta t)$ and $\psi_{ij}^n = \psi(x_i, y_j, n\Delta t)$, where $(x_i, y_j) = (ih, jh)$ for $i = 0, \ldots, N_x$ and $j = 0, \ldots, N_y$. The second-order accurate scheme is assumed as:

$$\frac{\phi^{n+1} - \phi^n}{\Delta t} = M_\phi \Delta\mu^{n+\frac{1}{2}}, \tag{12}$$

$$\mu^{n+\frac{1}{2}} = \frac{1}{2} \left(W_\phi(\hat{\phi}^{n+\frac{1}{2}}, \psi^{n+1}) + W_\phi(\hat{\phi}^{n+\frac{1}{2}}, \psi^n) \right) - \lambda_\phi \hat{\phi}^{n+\frac{1}{2}} + \lambda_\phi \phi^{n+\frac{1}{2}}$$

$$- \epsilon_\phi^2 \Delta\phi^{n+\frac{1}{2}} + \sigma\varphi^{n+\frac{1}{2}}, \tag{13}$$

$$\frac{\psi^{n+1} - \psi^n}{\Delta t} = M_\psi \Delta\nu^{n+\frac{1}{2}}, \tag{14}$$

$$\nu^{n+\frac{1}{2}} = \frac{1}{2} \left(W_\psi(\phi^{n+1}, \hat{\psi}^{n+\frac{1}{2}}) + W_\psi(\phi^n, \hat{\psi}^{n+\frac{1}{2}}) \right) - \lambda_\psi \hat{\psi}^{n+\frac{1}{2}} + \lambda_\psi \psi^{n+\frac{1}{2}}$$

$$- \epsilon_\psi^2 \Delta\psi^{n+\frac{1}{2}}, \tag{15}$$

where $\phi^{n+\frac{1}{2}}$ and $\hat{\phi}^{n+\frac{1}{2}}$ are defined as $\phi^{n+\frac{1}{2}} = (\phi^{n+1} + \phi^n)/2$ and $\hat{\phi}^{n+\frac{1}{2}} = (3\phi^n - \phi^{n-1})/2$, respectively; λ_ϕ and λ_ψ are two constant parameters; and $\bar{\phi} = \sum_{i=1}^{N_x} \sum_{j=1}^{N_y} \phi_{ij}^0 h^2/L^2$. Because of $-\Delta\varphi^{n+\frac{1}{2}} = \phi^{n+\frac{1}{2}} - \bar{\phi}$, Eqs. (12) and (13) are equivalent to the following equations:

$$\frac{\phi^{n+1} - \phi^n}{\Delta t} = M_\phi \Delta\mu^{n+\frac{1}{2}} - \sigma M_\phi \left(\frac{\phi^{n+1} + \phi^n}{2} - \bar{\phi} \right), \tag{16}$$

$$\mu^{n+\frac{1}{2}} = \frac{1}{2} \left(W_\phi(\hat{\phi}^{n+\frac{1}{2}}, \psi^{n+1}) + W_\phi(\hat{\phi}^{n+\frac{1}{2}}, \psi^n) \right) - \lambda_\phi \hat{\phi}^{n+\frac{1}{2}} + \lambda_\phi \phi^{n+\frac{1}{2}}$$

$$- \epsilon_\phi^2 \Delta\phi^{n+\frac{1}{2}} \tag{17}$$

Therefore, the stability of the system (12)–(13) and the system (16)–(17) are identical. Hence, we will only need to demonstrate the stability of the former, then solve the resulting scheme (16)–(17). Because of periodic boundary condition, we use the discrete Fourier transform operator $\mathcal{F}$ and inverse discrete Fourier transform operator $\mathcal{F}^{-1}$ to the coupled Cahn–Hilliard system:

$$\mathcal{F}(\phi_{pq}) = \sum_{i=0}^{N_x-1} \sum_{j=0}^{N_y-1} \phi_{ij} \exp^{-\sqrt{-1}(x_i\alpha_p + y_j\beta_q)} \text{ and } \mathcal{F}^{-1}(\phi_{ij})$$

$$= \sum_{p=0}^{N_x-1} \sum_{q=0}^{N_y-1} \phi_{pq} \exp^{\sqrt{-1}(x_i\alpha_p + y_j\beta_p)}.$$

The variables α_p and β_q are defined as $\alpha_p = 2\pi p/L_x$ and $\beta_q = 2\pi q/L_y$ for $p = 0, \ldots, N_x - 1$ and $q = 1, \ldots, N_y - 1$, respectively. Thus, by defining $A_{pq} = -[(\alpha_p\pi)^2 + (\beta_q\pi)^2]$, the discrete Fourier transform for the Laplacian operator can be defined as $\mathcal{F}(\Delta\phi_{pq}) = A_{pq}\mathcal{F}(\phi_{pq})$. Hence, we

can transform Eqs. (14)–(17) into the discrete Fourier space like this:

$$
\begin{pmatrix}
2 + \Delta t \sigma M_\phi & -2\Delta t M_\phi A_{pq} & 0 & 0 \\
-\lambda_\phi + \epsilon_\phi^2 A_{pq} & 2 & 0 & 0 \\
0 & 0 & 2 & -2\Delta t M_\psi A_{pq} \\
0 & 0 & -\lambda_\psi + \epsilon_\psi^2 A_{pq} & 2
\end{pmatrix}
$$

$$
\times
\begin{pmatrix}
\mathcal{F}(\phi_{pq}^{n+1,m+1}) \\
\mathcal{F}(\mu_{pq}^{n+1,m+1}) \\
\mathcal{F}(\psi_{pq}^{n+1,m+1}) \\
\mathcal{F}(v_{pq}^{n+1,m+1})
\end{pmatrix}
$$

$$
=
\begin{pmatrix}
\mathcal{F}\left(2\phi_{pq}^n - \Delta t \sigma M_\phi(\phi_{pq}^n - 2\bar\phi)\right) \\
\mathcal{F}\left(W_\phi(\hat\phi_{pq}^{n+\frac{1}{2}}, \psi_{pq}^{n+1,m}) + W_\phi(\hat\phi_{pq}^{n+\frac{1}{2}}, \psi_{pq}^n) - 2\lambda_\phi \hat\phi_{pq}^{n+\frac{1}{2}} + \lambda_\phi \phi_{pq}^n\right) \\
\mathcal{F}\left(2\phi_{pq}^n\right) \\
\mathcal{F}\left(W_\psi(\phi_{pq}^{n+1,m}, \hat\psi_{pq}^{n+\frac{1}{2}}) + W_\psi(\phi_{pq}^n, \hat\psi_{pq}^{n+\frac{1}{2}}) - 2\lambda_\psi \hat\psi_{pq}^{n+\frac{1}{2}} + \lambda_\psi \psi_{pq}^n\right)
\end{pmatrix}
\quad (18)
$$

Here, we have used the iterative method for $m = 0, 1, \dots$. It is obvious that $\phi^{n+1,m} = \mathcal{F}^{-1}(\mathcal{F}(\phi^{n+1,m}))$ and $\psi^{n+1,m} = \mathcal{F}^{-1}(\mathcal{F}(\psi^{n+1,m}))$. By setting $\phi^{n+1,0} = 2\phi^n - \phi^{n-1}$ and $\psi^{n+1,0} = 2\psi^n - \psi^{n-1}$, we solve Eq. (18) and set $\phi^{n+1} = \phi^{n+1,m+1}$ and $\psi^{n+1} = \psi^{n+1,m+1}$ until the consecutive error's relative L_2-norm $\|\phi^{n+1,m+1} - \phi^{n+1,m}\|_{L_2}/\|\phi^{n+1,m}\|_{L_2} + \|\psi^{n+1,m+1} - \psi^{n+1,m}\|_{L_2}/\|\psi^{n+1,m}\|_{L_2}$ is less than a given tolerance. The residual error converges rather quickly to a tolerance $1e$-5 in several iterations. Furthermore, GPU-accelerated discrete transform implementation can apply to the proposed numerical scheme straightforwardly, and the execution speed is many times faster than the alternative solution using only the CPU.

Lemma 1. If $\phi^n, \phi^{n-1}, \psi^n, \psi^{n-1}, \phi^{n+1}$, and ψ^{n+1} are the solutions of the scheme (12)–(15), then there exists $\hat\xi^{n+1}, \check\xi^{n+1}, \hat\zeta^{n+1}, \check\zeta^{n+1}$ such that:

$$
\frac{1}{2}\left(W_\phi(\hat\phi^{n+\frac{1}{2}}, \psi^{n+1}), \phi^{n+1} - \phi^n\right)_{L^2} + \frac{1}{2}\left(W_\phi(\hat\phi^{n+\frac{1}{2}}, \psi^n), \phi^{n+1} - \phi^n\right)_{L^2}
$$
$$
+ \frac{1}{2}\left(W_\psi(\phi^{n+1}, \hat\psi^{n+\frac{1}{2}}), \psi^{n+1} - \psi^n\right)_{L^2} + \frac{1}{2}\left(W_\psi(\phi^n, \hat\psi^{n+\frac{1}{2}}), \psi^{n+1} - \psi^n\right)_{L^2}
$$
$$
= \left(W(\phi^{n+1}, \psi^{n+1}) - W(\phi^n, \psi^n), \mathbf{1}\right)_{L^2}
$$
$$
- \frac{W_{\phi\phi}(\hat\xi^{n+1}, \check\zeta^{n+1})}{2}\left(\phi^{n+1} - \phi^n, \phi^{n+1} - 2\phi^n + \phi^{n-1}\right)_{L^2}
$$
$$
- \frac{W_{\psi\psi}(\check\xi^{n+1}, \hat\zeta^{n+1})}{2}\left(\psi^{n+1} - \psi^n, \psi^{n+1} - 2\psi^n + \psi^{n-1}\right)_{L^2}. \quad (19)
$$

Here, $W_{\phi\phi}$ and $W_{\psi\psi}$ are the second derivatives of the function W in regard to ϕ and ψ, respectively. $\sup(w_{\phi\phi})$ and $\sup(w_{\psi\psi})$ are the least upper bounds of $w_{\phi\phi}$ and $w_{\psi\psi}$, respectively.

Proof. According to the Taylor expansion, there exist two constants ξ_1^{n+1} and ξ_1^n which make the following expressions hold:

$$
\left(W(\phi^{n+1}, \psi^{n+1}), \mathbf{1}\right)_{L^2} = \left(W(\hat\phi^{n+\frac{1}{2}}, \psi^{n+1}), \mathbf{1}\right)_{L^2}
$$
$$
+ \left(W_\phi(\hat\phi^{n+\frac{1}{2}}, \psi^{n+1}), \phi^{n+1} - \hat\phi^{n+\frac{1}{2}}\right)_{L^2}
$$
$$
+ \frac{W_{\phi\phi}(\xi_1^{n+1}, \psi^{n+1})}{2}\|\phi^{n+1} - \hat\phi^{n+\frac{1}{2}}\|_{L^2}^2, \quad (20)
$$

$$
\left(W(\phi^n, \psi^{n+1}), \mathbf{1}\right)_{L^2} = \left(W(\hat\phi^{n+\frac{1}{2}}, \psi^{n+1}), \mathbf{1}\right)_{L^2}
$$
$$
+ \left(W_\phi(\hat\phi^{n+\frac{1}{2}}, \psi^{n+1}), \phi^n - \hat\phi^{n+\frac{1}{2}}\right)_{L^2}
$$
$$
+ \frac{W_{\phi\phi}(\xi_1^n, \psi^{n+1})}{2}\|\phi^n - \hat\phi^{n+\frac{1}{2}}\|_{L^2}^2. \quad (21)
$$

Combining Eqs. (20) and (21), there exists $\hat\xi_1^{n+1}$ such that the first left term in Eq. (19) can be expanded as:

$$
\left(W_\phi(\hat\phi^{n+\frac{1}{2}}, \psi^{n+1}), \phi^{n+1} - \phi^n\right)_{L^2} = \left(W(\phi^{n+1}, \psi^{n+1}) - W(\phi^n, \psi^{n+1}), \mathbf{1}\right)_{L^2}
$$
$$
- \frac{W_{\phi\phi}(\hat\xi_1^{n+1}, \psi^{n+1})}{2}
$$

$$
\times \left(\phi^{n+1} - \phi^n, \phi^{n+1} - 2\phi^n + \phi^{n-1}\right)_{L^2}. \quad (22)
$$

Similarly, another three terms in the left of Eq. (19) can be obtained as:

$$
\left(W_\phi(\hat\phi^{n+\frac{1}{2}}, \psi^n), \phi^{n+1} - \phi^n\right)_{L^2} = \left(W(\phi^{n+1}, \psi^n) - W(\phi^n, \psi^n), \mathbf{1}\right)_{L^2}
$$
$$
- \frac{W_{\phi\phi}(\hat\xi_2^{n+1}, \psi^n)}{2}
$$
$$
\times \left(\phi^{n+1} - \phi^n, \phi^{n+1} - 2\phi^n + \phi^{n-1}\right)_{L^2}, \quad (23)
$$

$$
\left(W_\psi(\phi^{n+1}, \hat\psi^{n+\frac{1}{2}}), \psi^{n+1} - \psi^n\right)_{L^2} = \left(W(\phi^{n+1}, \psi^{n+1}) - W(\phi^{n+1}, \psi^n), \mathbf{1}\right)_{L^2}
$$
$$
- \frac{W_{\psi\psi}(\phi^{n+1}, \hat\zeta_1^{n+1})}{2}
$$
$$
\times \left(\psi^{n+1} - \psi^n, \psi^{n+1} - 2\psi^n + \psi^{n-1}\right)_{L^2}, \quad (24)
$$

$$
\left(W_\psi(\phi^n, \hat\psi^{n+\frac{1}{2}}), \psi^{n+1} - \psi^n\right)_{L^2} = \left(W(\phi^n, \psi^{n+1}) - W(\phi^n, \psi^n), \mathbf{1}\right)_{L^2}
$$
$$
- \frac{W_{\psi\psi}(\phi^n, \hat\zeta_2^{n+1})}{2}
$$
$$
\times \left(\psi^{n+1} - \psi^n, \psi^{n+1} - 2\psi^n + \psi^{n-1}\right)_{L^2}. \quad (25)
$$

Because of the properties of continuous function, by combining Eqs. (22)–(25), there exist constants $\hat\xi^{n+1}, \check\xi^{n+1}, \hat\zeta^{n+1}, \check\zeta^{n+1}$ satisfying the following equation:

$$
\frac{1}{2}\left(W_\phi(\hat\phi^{n+\frac{1}{2}}, \psi^{n+1}), \phi^{n+1} - \phi^n\right)_{L^2} + \frac{1}{2}\left(W_\phi(\hat\phi^{n+\frac{1}{2}}, \psi^n), \phi^{n+1} - \phi^n\right)_{L^2}
$$
$$
+ \frac{1}{2}\left(W_\psi(\phi^{n+1}, \hat\psi^{n+\frac{1}{2}}), \psi^{n+1} - \psi^n\right)_{L^2} + \frac{1}{2}\left(W_\psi(\phi^n, \hat\psi^{n+\frac{1}{2}}), \psi^{n+1} - \psi^n\right)_{L^2}
$$
$$
= \left(W(\phi^{n+1}, \psi^{n+1}) - W(\phi^n, \psi^n), \mathbf{1}\right)_{L^2}
$$
$$
- \frac{W_{\phi\phi}(\hat\xi_1^{n+1}, \psi^n) + W_{\phi\phi}(\hat\xi_2^{n+1}, \psi^{n+1})}{4}\left(\phi^{n+1} - \phi^n, \phi^{n+1} - 2\phi^n + \phi^{n-1}\right)_{L^2}
$$
$$
- \frac{W_{\psi\psi}(\phi^{n+1}, \hat\zeta_1^{n+1}) + W_{\psi\psi}(\phi^n, \hat\zeta_2^{n+1})}{4}\left(\psi^{n+1} - \psi^n, \psi^{n+1} - 2\psi^n + \psi^{n-1}\right)_{L^2}
$$
$$
= \left(W(\phi^{n+1}, \psi^{n+1}) - W(\phi^n, \psi^n), \mathbf{1}\right)_{L^2}
$$
$$
- \frac{W_{\phi\phi}(\hat\xi^{n+1}, \check\zeta^{n+1})}{4}\left(\phi^{n+1} - \phi^n, \phi^{n+1} - 2\phi^n + \phi^{n-1}\right)_{L^2}
$$
$$
- \frac{W_{\psi\psi}(\check\xi^{n+1}, \hat\zeta^{n+1})}{4}\left(\psi^{n+1} - \psi^n, \psi^{n+1} - 2\psi^n + \psi^{n-1}\right)_{L^2}. \quad \square \quad (26)
$$

Then, we discretize the total energy functional (12)–(15) as:

$$
\mathcal{E}^d(\phi^n, \psi^n) = \left(W(\phi^n, \psi^n), \mathbf{1}\right) + \frac{\epsilon_\phi^2}{2}\|\nabla\phi^n\|_{L^2}^2
$$
$$
+ \frac{\epsilon_\psi^2}{2}\|\nabla\psi^n\|_{L^2}^2 + \frac{\sigma}{2}\|\nabla\varphi^n\|_{L^2}^2. \quad (27)
$$

Here, $\mathbf{1}$ is a vector and all entries are equivalent to 1. Then the discrete pseudo energy is defined as

$$
\bar{\mathcal{E}}^d(\phi^{n+1}, \phi^n, \psi^{n+1}, \psi^n) = \mathcal{E}^d(\phi^{n+1}, \psi^{n+1})
$$
$$
+ \frac{1}{8}\left(2\lambda_\phi - W_{\phi\phi}(\hat\xi^{n+1}, \check\zeta^{n+1})\right)\|\phi^{n+1} - \phi^n\|_{L^2}^2
$$
$$
+ \frac{1}{8}\left(2\lambda_\psi - W_{\psi\psi}(\check\xi^{n+1}, \hat\zeta^{n+1})\right)\|\psi^{n+1} - \psi^n\|_{L^2}^2. \quad (28)
$$

Lemma 2. Under the conditions $\lambda_\phi \geq \frac{1}{2}\sup(w_{\phi\phi})$ and $\lambda_\psi \geq \frac{1}{2}\sup(w_{\psi\psi})$, the solutions ϕ^{n+1} and ψ^{n+1} of Eqs. (12)–(15) satisfy:

$$
\mathcal{E}^d(\phi^{n+1}, \psi^{n+1}) \leq \bar{\mathcal{E}}^d(\phi^{n+1}, \phi^n, \psi^{n+1}, \psi^n). \quad (29)
$$

Proof. According to Eq. (28), we can obtain

$$
\mathcal{E}^d(\phi^{n+1}, \psi^{n+1}) - \bar{\mathcal{E}}^d(\phi^{n+1}, \phi^n, \psi^{n+1}, \psi^n) = -\frac{1}{8}\left(2\lambda_\phi - W_{\phi\phi}(\hat\xi^{n+1}, \check\zeta^{n+1})\right)
$$

$$\times \|\phi^{n+1} - \phi^n\|_{L^2}^2$$

$$- \frac{1}{8}\left(2\lambda_\psi - W_{\psi\psi}(\xi^{n+1}, \hat{\zeta}^{n+1})\right)$$

$$\times \|\psi^{n+1} - \psi^n\|_{L^2}^2 \leq 0. \quad \square \tag{30}$$

Theorem 1. *If $\lambda_\phi \geq \frac{1}{2}\sup(w_{\phi\phi})$ and $\lambda_\psi \geq \frac{1}{2}\sup(w_{\psi\psi})$, the scheme (12)–(15) satisfies the following discrete pseudo energy dissipation law:*

$$\bar{\mathcal{E}}^d(\phi^{n+1}, \phi^n, \psi^{n+1}, \psi^n) \leq \bar{\mathcal{E}}^d(\phi^n, \phi^{n-1}, \psi^n, \psi^{n-1}). \tag{31}$$

Proof. By applying the L^2 inner product of Eqs. (12) and (14) to $\mu^{n+\frac{1}{2}}$ and $\nu^{n+\frac{1}{2}}$ respectively, we obtain that

$$\left(\phi^{n+1} - \phi^n, \ \mu^{n+\frac{1}{2}}\right)_{L^2} = \Delta t M_\phi \left(\Delta \mu^{n+\frac{1}{2}}, \ \mu^{n+\frac{1}{2}}\right)_{L^2}$$
$$= -\Delta t M_\phi \|\nabla \mu^{n+\frac{1}{2}}\|_{L^2}^2, \tag{32}$$

$$\left(\psi^{n+1} - \psi^n, \ \nu^{n+\frac{1}{2}}\right)_{L^2} = \Delta t M_\psi \left(\Delta \nu^{n+\frac{1}{2}}, \ \nu^{n+\frac{1}{2}}\right)_{L^2}$$
$$= -\Delta t M_\psi \|\nabla \nu^{n+\frac{1}{2}}\|_{L^2}^2. \tag{33}$$

By employing the L^2 inner product of Eq. (13) to $\phi^{n+1} - \phi^n$ and employing the L^2 inner product of Eq. (15) to $\psi^{n+1} - \psi^n$, we have that

$$\left(\phi^{n+1} - \phi^n, \ \mu^{n+\frac{1}{2}}\right)_{L^2} = \frac{1}{2}\left(W_\phi(\hat{\phi}^{n+\frac{1}{2}}, \psi^{n+1})\right.$$
$$\left. + W_\phi(\hat{\phi}^{n+\frac{1}{2}}, \psi^n), \phi^{n+1} - \phi^n\right)_{L^2}$$
$$+ \lambda_\phi\left(\phi^{n+\frac{1}{2}} - \hat{\phi}^{n+\frac{1}{2}}, \phi^{n+1} - \phi^n\right)_{L^2} - \epsilon_\phi^2\left(\Delta\phi^{n+\frac{1}{2}}, \phi^{n+1} - \phi^n\right)_{L^2}$$
$$+ \sigma\left(\varphi^{n+\frac{1}{2}}, \phi^{n+1} - \phi^n\right)_{L^2}. \tag{34}$$

$$\left(\psi^{n+1} - \psi^n, \ \nu^{n+\frac{1}{2}}\right)_{L^2} = \frac{1}{2}\left(W_\psi(\phi^{n+1}, \hat{\psi}^{n+\frac{1}{2}})\right.$$
$$\left. + W_\psi(\phi^n, \hat{\psi}^{n+\frac{1}{2}}), \psi^{n+1} - \psi^n\right)_{L^2}$$
$$+ \lambda_\psi\left(\psi^{n+\frac{1}{2}} - \hat{\psi}^{n+\frac{1}{2}}, \psi^{n+1} - \psi^n\right)_{L^2} - \epsilon_\psi^2\left(\Delta\psi^{n+\frac{1}{2}}, \psi^{n+1} - \psi^n\right)_{L^2}. \tag{35}$$

By combing Eqs. (32)–(35), we have:

$$\frac{1}{2}\left(W_\phi(\hat{\phi}^{n+\frac{1}{2}}, \psi^{n+1}), \phi^{n+1} - \phi^n\right)_{L^2} + \frac{1}{2}\left(W_\phi(\hat{\phi}^{n+\frac{1}{2}}, \psi^n), \phi^{n+1} - \phi^n\right)_{L^2}$$
$$+ \frac{1}{2}\left(W_\psi(\phi^{n+1}, \hat{\psi}^{n+\frac{1}{2}}), \psi^{n+1} - \psi^n\right)_{L^2} + \frac{1}{2}\left(W_\psi(\phi^n, \hat{\psi}^{n+\frac{1}{2}}), \psi^{n+1} - \psi^n\right)_{L^2}$$
$$+ \lambda_\phi\left(\phi^{n+\frac{1}{2}} - \hat{\phi}^{n+\frac{1}{2}}, \phi^{n+1} - \phi^n\right)_{L^2} + \lambda_\psi\left(\psi^{n+\frac{1}{2}} - \hat{\psi}^{n+\frac{1}{2}}, \psi^{n+1} - \psi^n\right)_{L^2}$$
$$- \epsilon_\phi^2\left(\Delta\phi^{n+\frac{1}{2}}, \phi^{n+1} - \phi^n\right)_{L^2}$$
$$- \epsilon_\psi^2\left(\Delta\psi^{n+\frac{1}{2}}, \psi^{n+1} - \psi^n\right)_{L^2} + \sigma\left(\varphi^{n+\frac{1}{2}}, \phi^{n+1} - \phi^n\right)_{L^2}$$
$$= -\Delta t M_\phi \|\nabla\mu^{n+\frac{1}{2}}\|_{L^2}^2 - \Delta t M_\psi \|\nabla\nu^{n+\frac{1}{2}}\|_{L^2}^2. \tag{36}$$

For the first four terms of Eq. (36), we can use Lemma 1 and have:

$$\frac{1}{2}\left(W_\phi(\hat{\phi}^{n+\frac{1}{2}}, \psi^{n+1}), \phi^{n+1} - \phi^n\right)_{L^2} + \frac{1}{2}\left(W_\phi(\hat{\phi}^{n+\frac{1}{2}}, \psi^n), \phi^{n+1} - \phi^n\right)_{L^2}$$
$$+ \frac{1}{2}\left(W_\psi(\phi^{n+1}, \hat{\psi}^{n+\frac{1}{2}}), \psi^{n+1} - \psi^n\right)_{L^2} + \frac{1}{2}\left(W_\psi(\phi^n, \hat{\psi}^{n+\frac{1}{2}}), \psi^{n+1} - \psi^n\right)_{L^2}$$
$$= \left(W(\phi^{n+1}, \psi^{n+1}) - W(\phi^n, \psi^n), \mathbf{1}\right)_{L^2}$$
$$- \frac{W_{\phi\phi}(\hat{\xi}^{n+1}, \check{\zeta}^{n+1})}{4}\left(\phi^{n+1} - \phi^n, \phi^{n+1} - 2\phi^n + \phi^{n-1}\right)_{L^2}$$
$$- \frac{W_{\psi\psi}(\check{\xi}^{n+1}, \hat{\zeta}^{n+1})}{4}\left(\psi^{n+1} - \psi^n, \psi^{n+1} - 2\psi^n + \psi^{n-1}\right)_{L^2}. \tag{37}$$

For another terms of Eq. (36), we can obtain:

$$\lambda_\phi\left(\phi^{n+\frac{1}{2}} - \hat{\phi}^{n+\frac{1}{2}}, \phi^{n+1} - \phi^n\right)_{L^2} + \lambda_\psi\left(\psi^{n+\frac{1}{2}} - \hat{\psi}^{n+\frac{1}{2}}, \psi^{n+1} - \psi^n\right)_{L^2}$$
$$= \frac{\lambda_\phi}{2}\left(\phi^{n+1} - 2\phi^n + \phi^{n-1}, \phi^{n+1} - \phi^n\right)_{L^2}$$
$$+ \frac{\lambda_\psi}{2}\left(\psi^{n+1} - 2\psi^n + \psi^{n-1}, \psi^{n+1} - \psi^n\right)_{L^2}$$

$$= \frac{\lambda_\phi}{4}\left(\|\phi^{n+1} - \phi^n\|_{L^2}^2 - \|\phi^n - \phi^{n-1}\|_{L^2}^2 + \|\phi^{n+1} - 2\phi^n + \phi^{n-1}\|_{L^2}^2\right)_{L^2}$$
$$+ \frac{\lambda_\psi}{4}\left(\|\psi^{n+1} - \psi^n\|_{L^2}^2 - \|\psi^n - \psi^{n-1}\|_{L^2}^2\right.$$
$$\left. + \|\psi^{n+1} - 2\psi^n + \psi^{n-1}\|_{L^2}^2\right)_{L^2} \tag{38}$$

$$\epsilon_\phi^2\left(\Delta\phi^{n+\frac{1}{2}}, \phi^{n+1} - \phi^n\right)_{L^2} + \epsilon_\psi^2\left(\Delta\psi^{n+\frac{1}{2}}, \psi^{n+1} - \psi^n\right)_{L^2}$$
$$= -\frac{\epsilon_\phi^2}{2}\left(\nabla\phi^{n+1} + \nabla\phi^n, \nabla\phi^{n+1} - \nabla\phi^n\right)_{L^2}$$
$$- \frac{\epsilon_\psi^2}{2}\left(\nabla\psi^{n+1} + \nabla\psi^n, \nabla\psi^{n+1} - \nabla\psi^n\right)_{L^2}$$
$$= -\frac{\epsilon_\phi^2}{2}\left(\|\nabla\phi^{n+1}\|_{L^2}^2 - \|\nabla\phi^n\|_{L^2}^2\right) - \frac{\epsilon_\psi^2}{2}\left(\|\nabla\psi^{n+1}\|_{L^2}^2 - \|\nabla\psi^n\|_{L^2}^2\right) \tag{39}$$

$$\sigma\left(\varphi^{n+\frac{1}{2}}, \phi^{n+1} - \phi^n\right)_{L^2} = \frac{\sigma}{2}\left(\varphi^{n+1} + \varphi^n, \phi^{n+1} - \phi^n\right)_{L^2}$$
$$= \frac{\sigma}{2}\left(\varphi^{n+1} + \varphi^n, \phi^{n+1} - \bar{\phi} - (\phi^n - \bar{\phi})\right)_{L^2}$$
$$= -\frac{\sigma}{2}\left(\varphi^{n+1} + \varphi^n, \Delta\varphi^{n+1} - \Delta\varphi^n\right)_{L^2} = \frac{\sigma}{2}\left(\|\nabla\varphi^{n+1}\|_{L^2}^2 - \|\nabla\varphi^n\|_{L^2}^2\right). \tag{40}$$

Therefore, by Eqs. (28), (36)–(40), we obtain:

$$\bar{\mathcal{E}}^d(\phi^{n+1}, \phi^n, \psi^{n+1}, \psi^n) - \bar{\mathcal{E}}^d(\phi^n, \phi^{n-1}, \psi^n, \psi^{n-1})$$
$$= \mathcal{E}^d(\phi^{n+1}, \psi^{n+1}) - \mathcal{E}^d(\phi^n, \psi^n)$$
$$+ \frac{1}{8}\left(2\lambda_\phi - W_{\phi\phi}(\hat{\xi}^{n+1}, \check{\zeta}^{n+1})\right)\|\phi^{n+1} - \phi^n\|_{L^2}^2$$
$$- \frac{1}{8}\left(2\lambda_\phi - W_{\phi\phi}(\hat{\xi}^{n+1}, \check{\zeta}^{n+1})\right)\|\phi^n - \phi^{n-1}\|_{L^2}^2$$
$$+ \frac{1}{8}\left(2\lambda_\psi - W_{\psi\psi}(\check{\xi}^{n+1}, \hat{\zeta}^{n+1})\right)\|\psi^{n+1} - \psi^n\|_{L^2}^2$$
$$- \frac{1}{8}\left(2\lambda_\psi - W_{\psi\psi}(\check{\xi}^{n+1}, \hat{\zeta}^{n+1})\right)\|\psi^n - \psi^{n-1}\|_{L^2}^2$$
$$= -\Delta t M_\phi \|\nabla\mu^{n+\frac{1}{2}}\|_{L^2}^2 - \frac{\left(2\lambda_\phi - W_{\phi\phi}(\hat{\xi}^{n+1}, \check{\zeta}^{n+1})\right)}{8}\|\phi^{n+1} - 2\phi^n + \phi^{n-1}\|_{L^2}^2$$
$$- \Delta t M_\psi \|\nabla\nu^{n+\frac{1}{2}}\|_{L^2}^2 - \frac{\left(2\lambda_\psi - W_{\psi\psi}(\check{\xi}^{n+1}, \hat{\zeta}^{n+1})\right)}{8}$$
$$\times \|\psi^{n+1} - 2\psi^n + \psi^{n-1}\|_{L^2}^2 \leq 0 \quad \square \tag{41}$$

Theorem 2. *Suppose that $\phi^0 = \phi^{-1}$, $\psi^0 = \psi^{-1}$, then the discrete total energy defined in (27) satisfies that*

$$\mathcal{E}^d(\phi^{n+1}, \psi^{n+1}) \leq \bar{\mathcal{E}}^d(\phi^{n+1}, \phi^n, \psi^{n+1}, \psi^n) \leq \mathcal{E}^d(\phi^0, \psi^0). \tag{42}$$

Proof. According to Lemma 1 and Theorem 1, we have a chain of inequalities,

$$\mathcal{E}^d(\phi^{n+1}, \psi^{n+1}) \leq \bar{\mathcal{E}}^d(\phi^{n+1}, \phi^n, \psi^{n+1}, \psi^n) \leq \bar{\mathcal{E}}^d(\phi^n, \phi^{n-1}, \psi^n, \psi^{n-1}) \leq \dots$$
$$\leq \bar{\mathcal{E}}^d(\phi^0, \phi^{-1}, \psi^0, \psi^{-1})$$
$$= \mathcal{E}^d(\phi^0, \psi^0). \quad \square \tag{43}$$

In our proof, the stabilizing parameter λ_ϕ and λ_ψ are chosen to be $\lambda_\phi \geq \frac{1}{2}\sup(w_{\phi\phi})$ and $\lambda_\psi \geq \frac{1}{2}\sup(w_{\psi\psi})$ to make the energy strictly non-increasing. Because $w_{\phi\phi} = \phi^3 - \phi + 2b\psi$ and $w_{\psi\psi} = \psi^3 - \psi$ are two quadratic functions, $\sup(w_{\phi\phi}) = 3\tilde{\phi}^2 - 1 + 2b\tilde{\psi}$ and $\sup(w_{\phi\phi}) = 3\tilde{\psi}^2 - 1$ are satisfied. Here, $\tilde{\phi}$ and $\tilde{\psi}$ are the maximum values of ϕ and ψ, respectively. For simplicity, we choose $\lambda_\phi = \lambda_\psi = 1 + b$ for the initial conditions $\phi^0 \in [-1, 1]$ and $\psi^0 \in [-1, 1]$.

4. Numerical experiments

In this Section, we perform several numerical experiments to demonstrate the accuracy and stability of the scheme we proposed. To insure the second-order accuracy of every time step, the good initial steps ϕ^{-1} and ψ^{-1} are required. For the sake of simplicity, we suppose that $\phi^0 = \phi^{-1}$ and $\psi^0 = \psi^{-1}$. Though it leads to a loss of accuracy in the
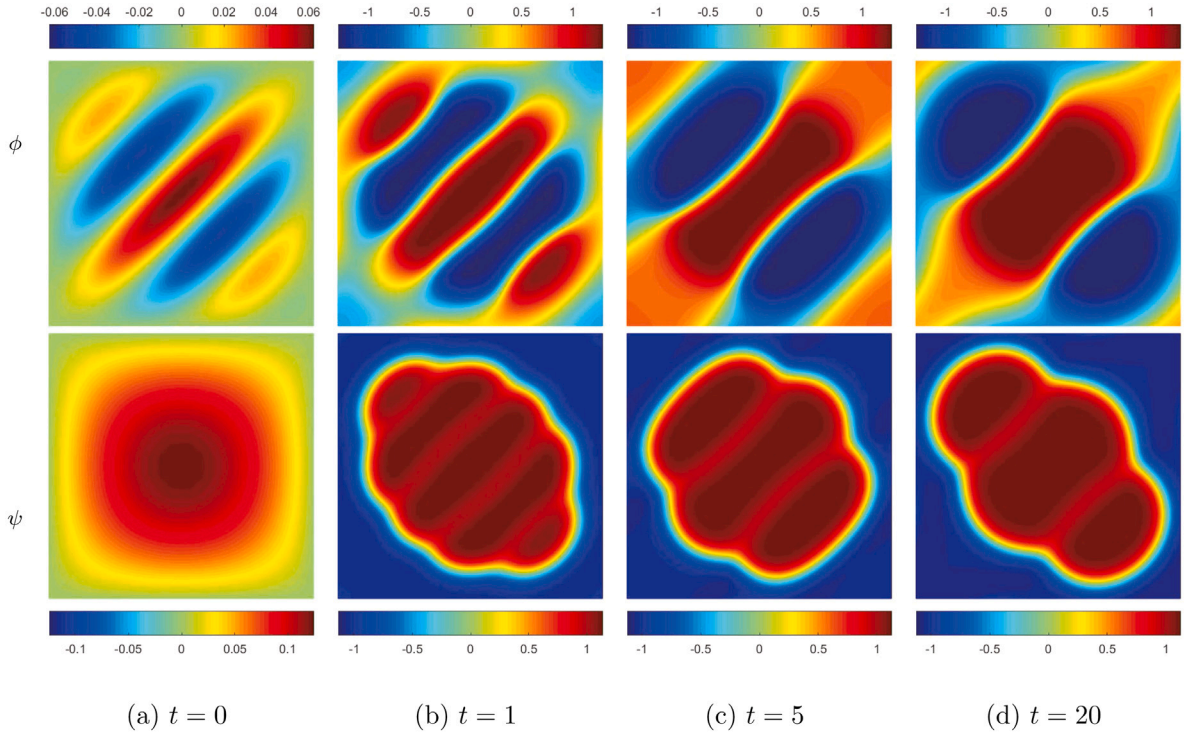
Fig. 1. Evolutions of ϕ (top) and ψ (bottom). The computational times are listed below each figure.
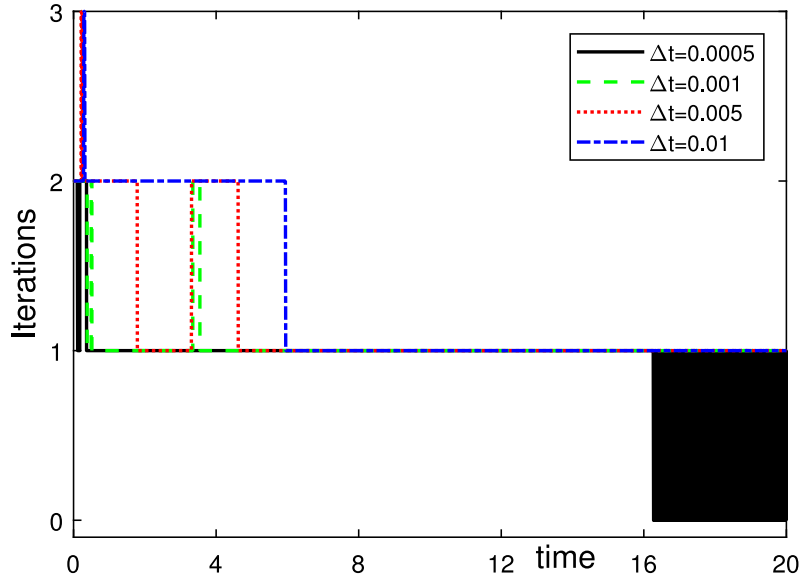

Fig. 2. The number of iterations with different time steps.

initial time step, the proposed scheme satisfies second order accuracy in later calculations. Therefore, we can observe a second-order accuracy in regard to time and space for a long simulation.

4.1. Evolution of phase separation

In this test, we begin with a computational simulation to explain the microphase and macrophase separations' evolution in two-dimensional space. The initial conditions are set as $M_\phi = 0.05$, $M_\psi = 1$, $a = 0.01$, $b = -0.3$, $\phi(x, y, 0) = \cos(10(x - y))x(x - 1)y(y - 1)$, $\psi(x, y, 0) = \sin(2x(x - 1)y(y - 1))$ on the domain $(0, 1) \times (0, 1)$ with a mesh grid 128×128. Here, $\epsilon_\phi = \epsilon_\psi = 0.03$, and $\sigma = 0$ are adopted. The calculation runs until $T = 20$ with $\Delta t = 0.001$. The evolution of ϕ and ψ in two-dimensional

space are shown in Fig. 1. The blue domain in the snapshots of ψ corresponds the homopolymer rich domain, the red domain of ψ corresponds the copolymer rich domain. By observing ϕ, we can see that in the copolymer rich domain, $A - B$ diblock copolymers evolve into a layered structure. In Fig. 3, the evolution of the discrete energies $\mathcal{E}(\phi, \psi)$ are shown with several time steps $\Delta t = 0.0005$, 0.001, 0.005, and 0.01. We discover that the evolution of energy decreases faster when there is a smaller time step. As mentioned in the above, the iterative method is introduced to solve numerical solutions in Eqs. (12)–(15). By setting $\phi^{n+1,0} = 2\phi^n - \phi^{n-1}$ and $\psi^{n+1,0} = 2\psi^n - \psi^{n-1}$, we solve Eqs. (12)–(15) and set $\phi^{n+1} = \phi^{n+1,m+1}$ and $\psi^{n+1} = \psi^{n+1,m+1}$ until a relative L_2-norm of the consecutive error $\|\phi^{n+1,m+1} - \phi^{n+1,m}\|_{L_2}/\|\phi^{n+1,m}\|_{L_2} + \|\psi^{n+1,m+1} -$
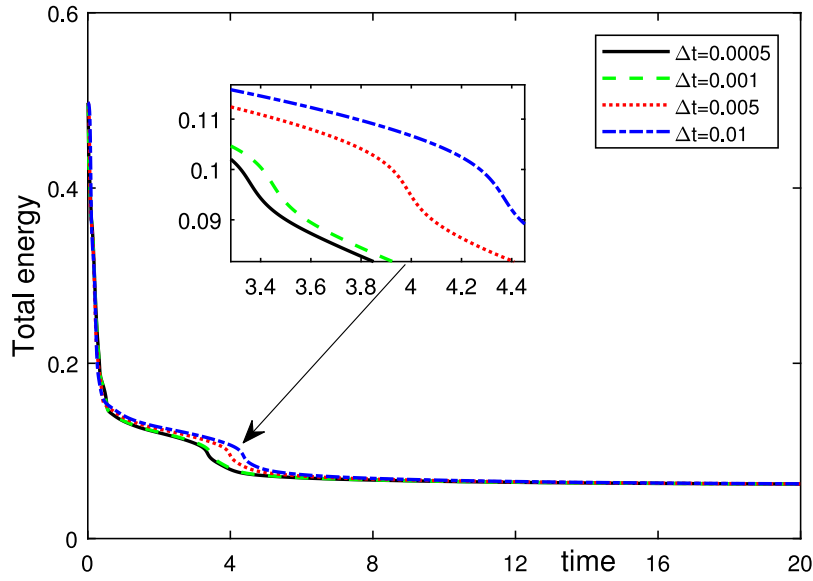
Fig. 3. The evolution of the discrete energy $\mathcal{E}$ with different time steps.

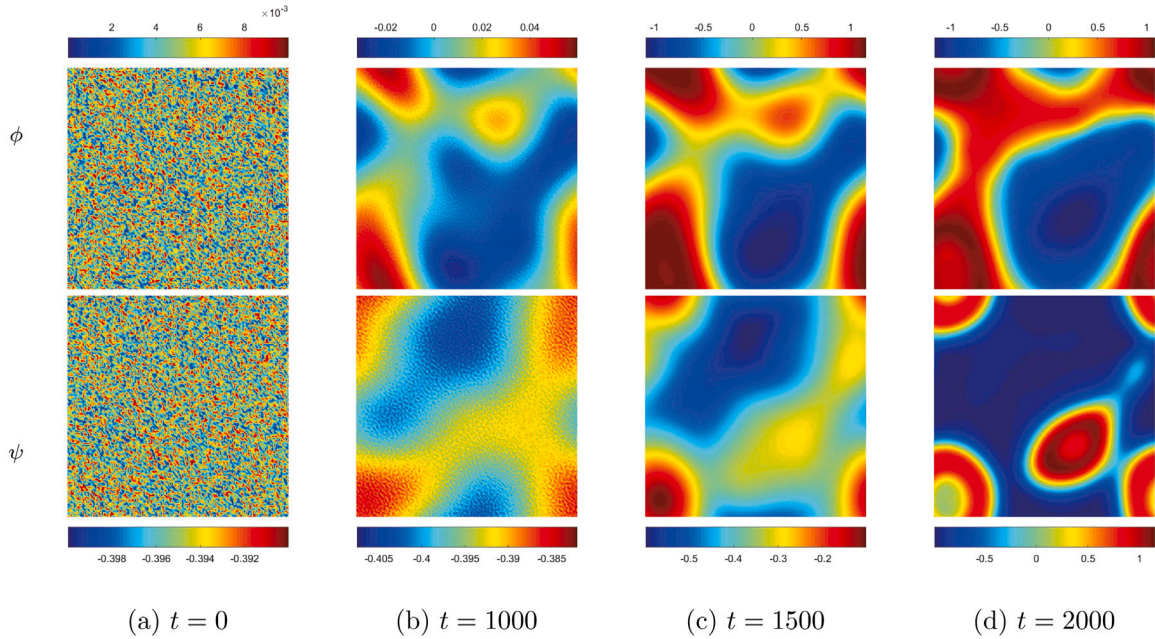(a) $t = 0$ (b) $t = 1000$ (c) $t = 1500$ (d) $t = 2000$

Fig. 4. Evolution of ϕ (top) and ψ (bottom). The parameters are $\epsilon_\phi = \epsilon_\psi = 0.04$, $M_\phi = 0.05$, $M_\psi = 1$, $a = 0.01$, $b = -0.1$, $\sigma = 0$, and $\Delta t = 100$. The time is shown below each figure.

$\psi^{n+1,m}\|_{L_2}/\|\psi^{n+1,m}\|_{L_2}$ is less than a given tolerance $1e$-5. Fig. 2 shows the number of iterations with different time steps. Observing these results, we can see that the residual error converges rather quickly to the given tolerance in few iterations.

4.2. Stability of the proposed scheme

In this test, the stability of the proposed scheme is investigated with random initial conditions $\phi(x, y, 0) = 0.01\text{rand}(x, y)$, $\psi(x, y, 0) = -0.4 + 0.01\text{rand}(x, y)$ on the domain $(0, 1) \times (0, 1)$ with a mesh grid 128×128. The rand(x,y) is a random number within the range of $[-1, 1]$. Here, $M_\phi = 0.05$, $M_\psi = 1$, $a = 0.01$, $b = -0.1$, $\epsilon_\phi = \epsilon_\psi = 0.04$, and $\sigma = 0$ are used. We run the calculation until $T = 2000$ with a larger time step $\Delta t = 100$. The evolutions of ϕ and ψ in two-dimensional space are shown in Fig. 4. It should be noted that since our scheme is nonlinear, it is difficult to prove the existence and uniqueness of our solution. In

Fig. 5, we plot the evolutions of the pseudo energy and total energy with a larger time step $\Delta t = 100$. It can be seen that the numerical solution will not explode, which implies that the proposed scheme can use larger steps. While a large time step makes the evolution be less accurate due to the accuracy of our proposed method with respect to time. Therefore, to balance the relationship between accuracy and computational costs, an appropriate value for Δt is $0.1h$.

4.3. Convergence test

In this test, we demonstrate the prediction of spatial and temporal convergence by choosing the increasing finer grids $h = 1/2^n$ for $n = 5, 6, 7, 8$ and 9 in the domain $\Omega = (0, 1) \times (0, 1)$. We use the same initial condition as $\phi(x, y, 0) = \psi(x, y, 0) = 0.05 + 0.01(\sin(2\pi x) + \cos(2\pi y))$. We set $M_\phi = M_\psi = 1$, $a = 2$, $b = 3$, $\epsilon_\phi^2 = \epsilon_\psi^2 = 0.0625$, $\sigma = 50$. We run the simulation up to the time $T = 0.1$ with a time step $\Delta t = 0.1h$. Since there
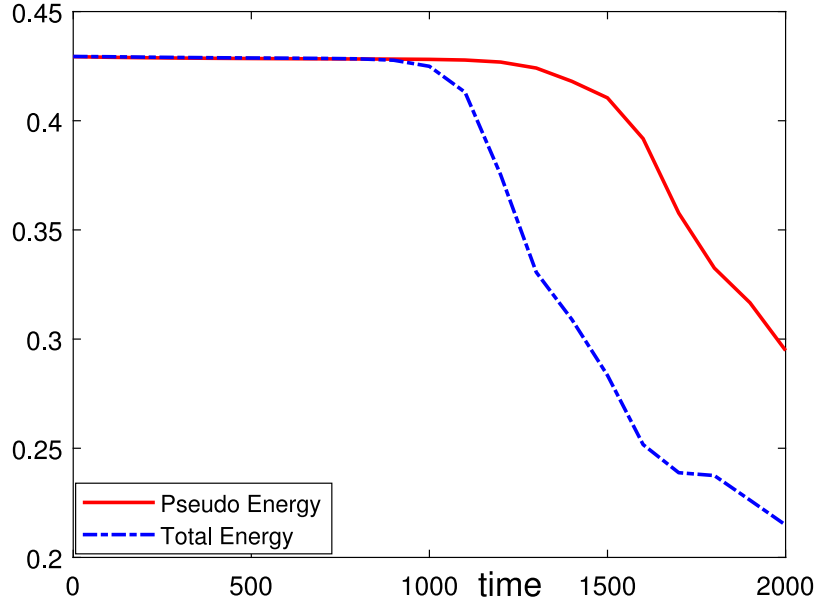
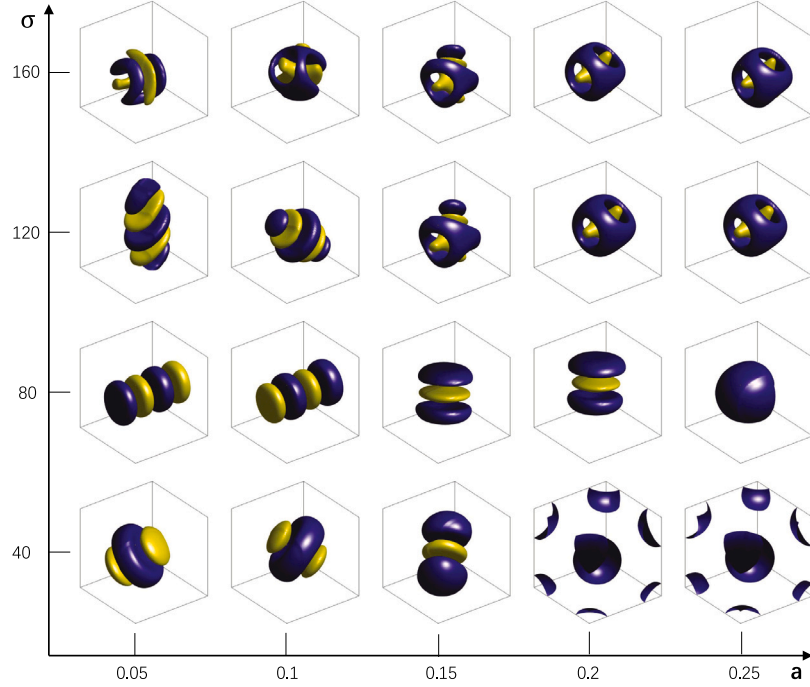**Fig. 5.** Temporal evolutions of pseudo energy and total energy with a larger time step $\Delta t = 100$.

Fig. 6. The phase diagram of ϕ at $T = 50$ for different parameters a and σ.

is no closed-form exact solution for this initial condition, we define the Cauchy error $e_{\phi(h/\frac{h}{2})}$ and $e_{\psi(h/\frac{h}{2})}$ between the computational solutions:

$$
e_{ij}^{\phi(h/\frac{h}{2})} = \phi_{ij}^h - \frac{(\phi_{2i-1,2j-1}^{h/2} + \phi_{2i-1,2j}^{h/2} + \phi_{2i,2j-1}^{h/2} + \phi_{2i,2j}^{h/2})}{4}
$$

$$
e_{ij}^{\psi(h/\frac{h}{2})} = \psi_{ij}^h - \frac{(\psi_{2i-1,2j-1}^{h/2} + \psi_{2i-1,2j}^{h/2} + \psi_{2i,2j-1}^{h/2} + \psi_{2i,2j}^{h/2})}{4}.
$$

The convergence rate is defined as $log_2(\|e_h\|_2/\|e_{\frac{h}{2}}\|_2)$, where $\|e\|_2^2$ is the discrete l_2-norm defined as $\|e\|_2^2 = \Sigma_{i=1}^{Nx} \Sigma_{j=1}^{Ny} e_{ij}^2/(NxNy)$. Because we refine the spatial and temporal grids by 2, the rate of successive errors should increase by 2. The errors and rates of second-order

convergence are presented in Table 1. As illustrated in Table 1, second-order accuracy with respect to the space is observed. Next, we fix the space step size as $h = 1/128$ and choose a set of time-steps $\Delta t = 0.016h$, $0.008h$, $0.004h$, $0.002h$, and $0.001h$. Computational solutions are calculated up to time $T = 0.01$. We define the Cauchy error of a grid to be

$$
e_{ij}^{\phi(\Delta t/\frac{\Delta t}{2})} = \phi_{ij}^{\Delta t} - \phi_{ij}^{\Delta t/2} \text{ and } e_{ij}^{\psi(\Delta t/\frac{\Delta t}{2})} = \psi_{ij}^{\Delta t} - \psi_{ij}^{\Delta t/2}.
$$

According to the definition above, we give the errors and convergence's rates in Table 2. Time-dependent second-order accuracy is observed, as expected by discretization.
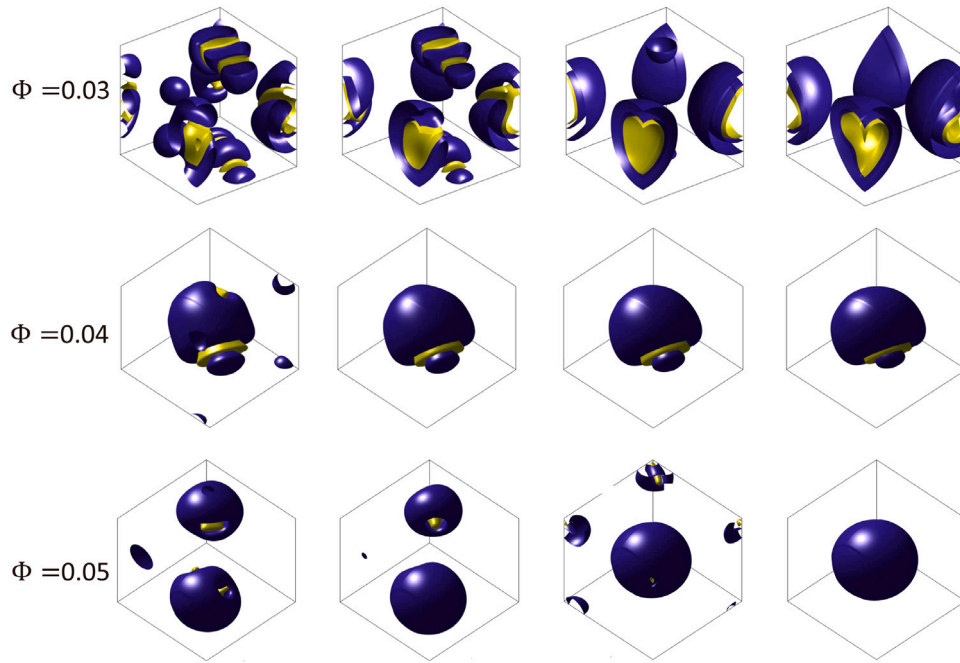
Fig. 7. Evolutions of ϕ with different ϵ_ψ. From left to right, the computational times are $t = 2.5, 5, 7,$ and 50, respectively.

(a) $\epsilon_\phi = 0.01$ (b) $\epsilon_\phi = 0.02$ (c) $\epsilon_\phi = 0.03$ (d) $\epsilon_\phi = 0.04$
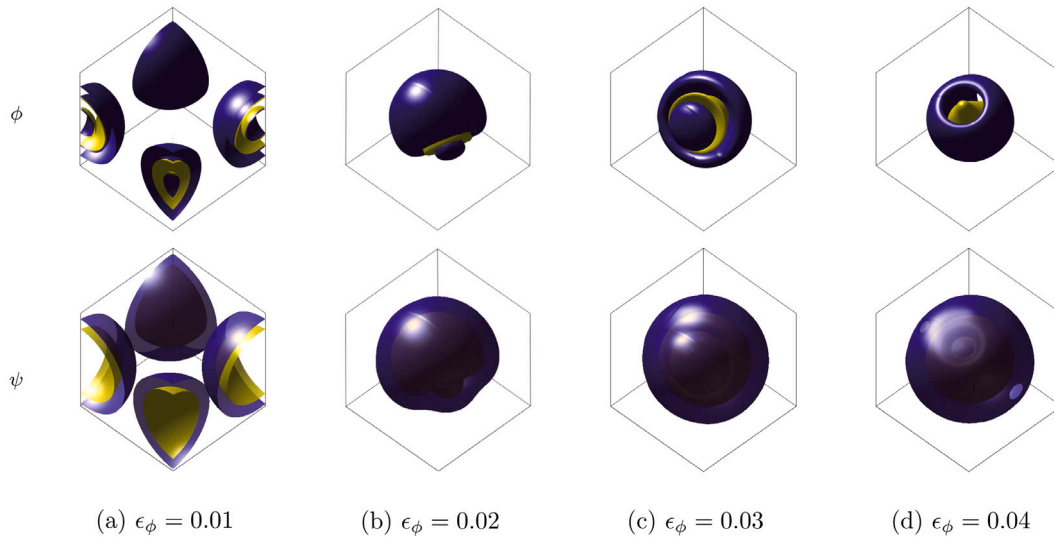
Fig. 8. Evolutions of ϕ and ψ with different parameter ϵ_ϕ.

Table 1
Errors and convergence rates with various mesh grids. $\Delta t = 0.1h$ is fixed.

h_c	h_f	$\|\phi_{h_c} - \phi_{h_f}\|_{L^2}$	Rate	$\|\psi_{h_c} - \psi_{h_f}\|_{L^2}$	Rate
32×32	64×64	$2.9235e{-}04$		$3.9307e{-}04$	
64×64	128×128	$7.2794e{-}05$	2.006	$9.7851e{-}05$	2.006
128×128	256×256	$1.8180e{-}05$	2.001	$2.4437e{-}05$	2.002
256×256	512×512	$4.5440e{-}06$	2.000	$6.1075e{-}06$	2.000

Table 2
Errors and convergence rates with various time steps. $h = 1/128$ is fixed.

Δt_c	Δt_f	$\|\phi_{\Delta t_c} - \phi_{\Delta t_f}\|_{L^2}$	Rate	$\|\psi_{h_c} - \psi_{h_f}\|_{L^2}$	Rate
$0.016h$	$0.008h$	$6.9986e{-}04$		$2.6182e{-}04$	
$0.008h$	$0.004h$	$1.9449e{-}04$	1.847	$7.2823e{-}05$	1.846
$0.004h$	$0.002h$	$4.8570e{-}05$	2.002	$1.8147e{-}05$	2.005
$0.002h$	$0.001h$	$1.2136e{-}05$	2.001	$4.5312e{-}06$	2.002

4.4. Effect of parameter a and σ

In this test, we will investigate the effect of parameters a and σ. Because the frustration effects are more noticeable in small system, we perform the numerical experiments on the domain $(0, 1) \times (0, 1) \times (0, 1)$ with a mesh grid $128 \times 128 \times 128$. The initial condition is set as $\phi(x, y, 0) = 0.01 rand(x, y, z)$, $\psi(x, y, 0) = -0.5 + 0.01 rand(x, y, z)$. Here,

$M_\phi = 0.05$, $M_\psi = 1$, $\epsilon_\phi = \epsilon_\psi = 0.04$, and $b = -0.5$. The numerical simulation runs until $T = 50$ with $\Delta t = 0.005$. In the evolution of microphase separation, the yellow and blue surfaces in the snapshots of ϕ represent the iso-surface of $\phi = 1$ and $\phi = -1$, respectively. From bottom to top, we can see that the interface area in the copolymer domain enlarges as the value of σ increases. Lamellar multilayer, micelle, vesicle, and multiples are common minimizers in the phase
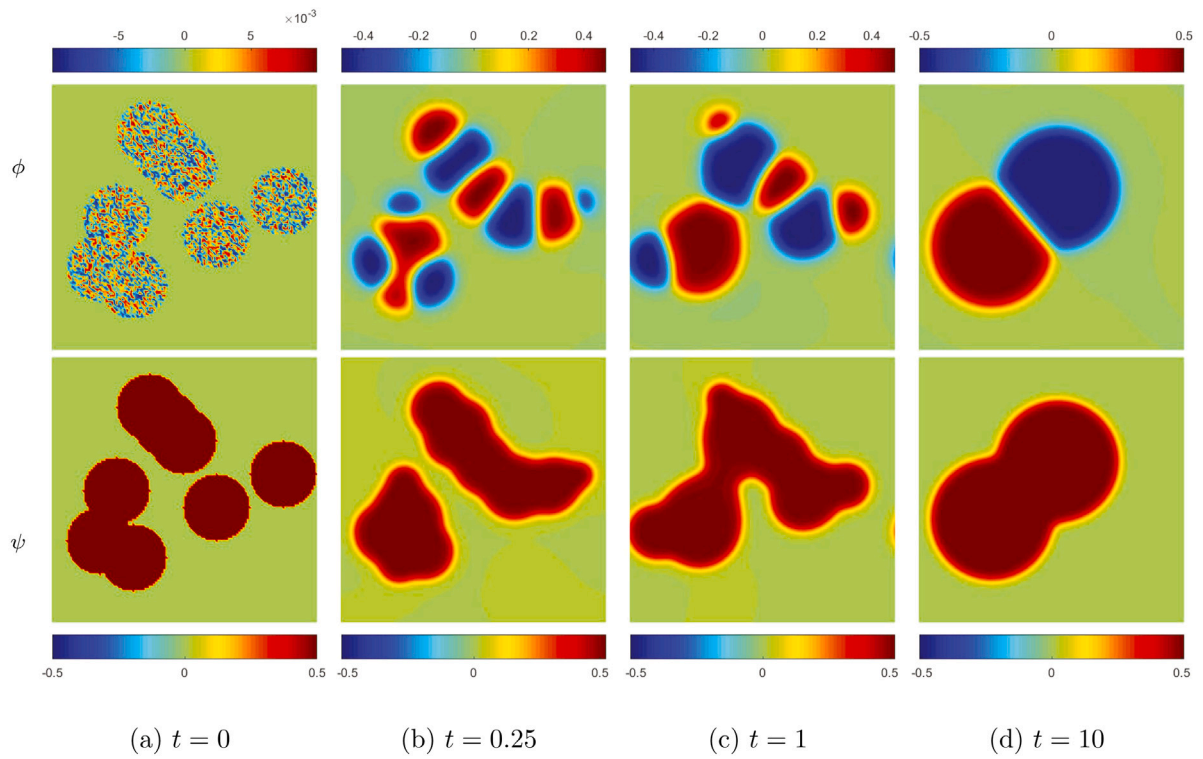
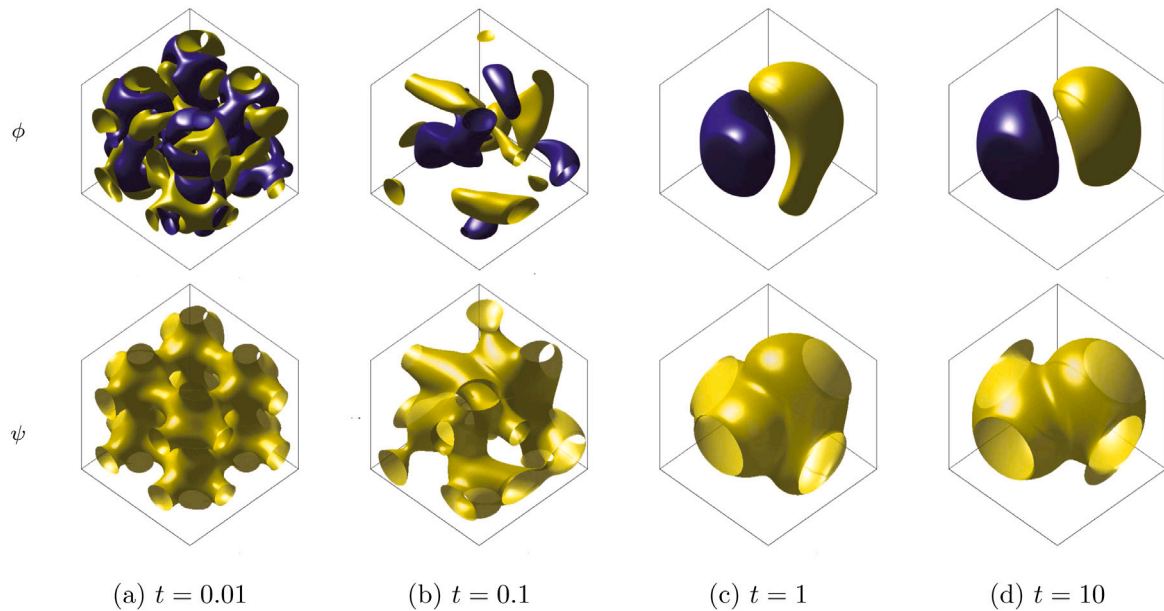**Fig. 9.** Evolutions of ϕ (top) and ψ (bottom) for copolymer solvent mixtures in two dimensional space.

Fig. 10. Evolutions of ϕ (top) and ψ (bottom) for copolymer solvent mixtures in three dimensional space.

diagram. Smaller σ and larger a lead to a smaller value of free energy. Commonly, the free energy of onion-like morphology is smaller than the multipod structure. The onion-like morphology in the lower right corner of Fig. 6 is consistent with the findings above. For a larger σ, the microstructures evolve from lamellar multilayer to multipods, tend towards a more stable structure.

4.5. Effect of parameter ϵ_ϕ and ϵ_ψ

ϵ_ϕ and ϵ_ψ increase with the thickness of components' propagating fronts. In this test, we study the effect of ϵ_ϕ and ϵ_ψ. The initial condition is set as $\phi(x, y, 0) = 0.01 rand(x, y, z)$, $\psi(x, y, 0) = -0.5 + 0.01 rand(x, y, z)$ on the domain $(0, 1) \times (0, 1) \times (0, 1)$ with a mesh grid $128 \times 128 \times 128$. Here, $M_\phi = 0.05$, $M_\psi = 1$, $a = 0.25$, $b = -0.5$, and $\sigma = 120$. We run the numerical simulation until $T = 50$ with a time step $\Delta t = 0.005$. Here, $\epsilon_\phi = 0.02$ is fixed and ϵ_ψ is set as 0.03, 0.04, and 0.05, respectively. In order to test ϵ_ϕ, we set $\epsilon_\phi = 0.01$, 0.02, 0.03, and 0.04 with the fixed parameter $\epsilon_\psi = 0.04$. In the evolution of microphase separation, the yellow and blue surfaces in the snapshots of ϕ represent the iso-surface of $\phi = 1$ and $\phi = -1$. In the evolution of macrophase separation, the yellow and blue surfaces in the snapshots of ψ represent the iso-surface

of $\psi = 1$ and $\psi = -1$. Fig. 7 shows the evolution of ϕ with different ϵ_ψ. Observing these results, we can see that in the copolymer domain of macrophase separation, the microstructure of ϕ evolutes from lamellar multilayer to onion-like morphology, the interface between copolymer and homopolymer is thicker with the increment of ϵ_ψ. Fig. 8(a)–(d) show the morphology of ϕ and ψ in $T = 50$ with different ϵ_ϕ. Through the comparison of different ϵ_ϕ, we can see that in the copolymer domain of macrophase separation, the microstructure of ϕ evolves from lamellar multilayer to multipod morphology, the interface between block A and B is a thinker with the increment of ϵ_ψ.

4.6. Copolymer solvent mixtures

In this test, we consider the copolymer solvent mixture by using $W = a\phi_A^2(1 - \phi_A)^2 + b\phi_B^2(1 - \phi_B)^2 + c\phi_S^2(1 - \phi_S)^2$ [38]. Here, ϕ_A, ϕ_B and ϕ_S denote the volume fractions of A-, B-, and S-diblock copolymer, respectively. The blocking ratio f defined by $f = N_A/(N_A + N_B)$, is the ratio of A-monomer compared with the total polymer volume, where N_A, N_B are the numbers of the corresponding monomers per molecule. For $\phi = (1 - f)\phi_A - f\phi_B$, $\psi = f\phi_A + (1 - f)\phi_B$, and the incompressibility $\phi_A + \phi_B + \phi_S = 1$, we can convert this equation into the form of ϕ and ψ. When $\phi = 0$ and $\psi = 0$, the potential $W(\phi, \psi)$ has minima, which is concomitant with pure solvent [51]. When $\phi + \psi = 1$ and one of them equals f, it corresponds to pure A or B monomer, respectively. Here, f is set as $f = 0.5$, therefore, $\psi = 0.5$, $\phi = 0.5$ and $\psi = 0.5$, $\phi = -0.5$ correspond to the block A and B respectively. $\phi = 0$, $\psi = 0.5$ and $\phi = 0$, $\psi = 0$ correspond to the copolymer rich domain and homopolymer rich domain respectively. We begin with a numerical simulation to show the evolution of microphase separation and macrophase separation in two-dimensional space. We set randomly four circular regions of radius $1/8$ on the domain $(0, 1) \times (0, 1)$ with a mesh grid 128×128. The initial conditions are set as $M_\phi = M_\psi = 1$, $a = b = c = 0.1$. We set $\phi(x, y, 0) = 0.02(rand(x, y) - 0.5)$, $\psi(x, y, 0) = 0.5$ within the region and $\phi(x, y, 0) = 0$, $\psi(x, y, 0) = 0$ outside the region. Here, $\epsilon_\phi = \epsilon_\psi = 0.01$, $\lambda_\phi = 0.5(10.5b - a)$, $\lambda_\psi = a + 13b + 52c$, and $\sigma = 0$ are used. The evolution of ϕ and ψ in two-dimensional space is shown in Fig. 9. The calculation is run until $T = 10$ with a time step $\Delta t = 0.001$. In Fig. 9, the green domain of ψ corresponds to the homopolymer rich domain, the red domain of ψ corresponds to the copolymer rich domain. We can see that in the copolymer rich domain, $A - B$ diblock copolymers evolve into a layered structure.

In the numerical simulation in three-dimensional space, to control the proportion of solvent in the entire space as a constant, we set randomly eight spherical area of radius $1/4$ on the domain $(0, 1) \times (0, 1) \times (0, 1)$ with a mesh grid $128 \times 128 \times 128$. In the evolution of microphase separation, the yellow and blue surfaces in the snapshots of ϕ corresponds to the iso-surface of $\phi = 0.5$ and $\phi = -0.5$. In the evolution of macrophase separation, the yellow surfaces in the snapshots of ψ corresponds to the iso-surface of $\psi = 0.5$. The experimental results are shown in Fig. 10. We can see that our method has a good performance in the simulation of numerical solution in three-dimensional space.

5. Conclusions

In this study, we developed a numerical method with second-order accuracy and unconditional energy stability for the coupled Cahn–Hilliard system for homopolymer and copolymer mixtures in two- and three-dimensional spaces. We proved the non-increasing of discrete energy by introducing pseudo energy. To efficiently solve the discrete system, we used a fast iterative Fourier transform method. We proved that our scheme is unconditional stable, therefore our scheme can use large time steps. We numerically investigated the stability and convergence of the proposed scheme. Several numerical experiments were performed to show a set of morphologies of pattern formations in the copolymer and homopolymer mixtures. The computational experiments confirmed the efficiency of the proposed scheme.

CRediT authorship contribution statement

Yibao Li: Methodology, Software, Investigation, Writing - original draft, Writing - review & editing. **Lujing Zhang:** Methodology, Investigation, Writing - original draft. **Qing Xia:** Software, Writing - original draft. **Qian Yu:** Validation, Visualization, Writing - original draft. **Junseok Kim:** Methodology, Supervision, Writing - Original Draft.

Declaration of competing interest

The authors declare that they have no known competing financial interests or personal relationships that could have appeared to influence the work reported in this paper.

References

[1] K.B. Glasner, Evolution and competition of block copolymer nanoparticles, SIAM J. Appl. Math. 79 (1) (2019) 28–54.

[2] K.I. Winey, E.L. Thomas, L.J. Fetters, Isothermal morphology diagrams for binary blends of diblock copolymer and homopolymer, Macromolecules 25 (10) (1992) 2645–2650.

[3] I.W. Hamley, The Physics of Block Copolymers, Oxford University Press, Oxford, 1998.

[4] P. Cumsille, J.A. Asenjo, C. Conca, A novel model for biofilm growth and its resolution by using the hybrid immersed interface-level set method, Comput. Math. Appl. 67 (1) (2014) 34–51.

[5] M. Abdolahzadeh, A. Tayebi, P. Omidvar, Mixing process of two-phase non-Newtonian fluids in 2D using Smoothed Particle Hydrodynamics, Comput. Math. Appl. 78 (1) (2019) 110–122.

[6] Y. Li, H. Zhang, M. Bao, Z. Wang, Dissipative particle dynamics simulation on the association between polymer and surfactant: Effects of surfactant and polymer feature, Comput. Mater. Sci. 63 (2012) 154–162.

[7] A.V. Ruzette, L. Leibler, Block copolymers in tomorrow's plastics, Nature Mater. 4 (2005) 19–31.

[8] A. Harada, K. Kataoka, Supramolecular assemblies of block copolymers in aqueous media as nanocontainers relevant to biological applications, Prog. Polym. Sci. 31 (11) (2006) 949–982.

[9] E. Waris, N. Ashammakhi, M. Lehtimaki, R.M. Tulamo, P. Toemala, M. Kellomaki, Y.T. Konttinen, Long-term bone tissue reaction to polyethylene oxide/polybutylene terephthalate copolymer (Polyactive(r)) in metacarpophalangeal joint reconstruction, Biomaterials 29 (16) (2008) 2509–2515.

[10] H. Bonnemann, R.M. Richards, Nanoscopic metal particles synthetic methods and potential applications, Eur. J. Inorg. Chem. (2001) 2455–2480.

[11] C. Alain, Y. Amina, P. Mathis, Lattice Boltzmann simulations of 3D crystal growth: Numerical schemes for a phase-field model with anti-trapping current, Comput. Math. Appl. 71 (9) (2016) 1784–1798.

[12] L. Dong, W. Feng, C. Wang, S.M. Wise, Z. Zhang, Convergence analysis and numerical implementation of a second order numerical scheme for the three-dimensional phase field crystal equation, Comput. Math. Appl. 75 (6) (2017) 1912–1928.

[13] P.C. Millett, Mesoscopic simulations of coarsening kinetics within block-copolymer/homopolymer thin films, Comput. Mater. Sci. 125 (2016) 20–27.

[14] B. Xia, C. Mei, Q. Yu, Y. Li, A second order unconditionally stable scheme for the modified phase field crystal model with elastic interaction and stochastic noise effect, Comput. Methods Appl. Mech. Engrg. 363 (2020) 112795.

[15] A.J. Archer, D.J. Ratliff, A.M. Rucklidge, P. Subramanian, Deriving phase field crystal theory from dynamical density functional theory: Consequences of the approximations, Phys. Rev. E 100 (2) (2019).

[16] A. Fakhari, M. Geier, D. Bolster, A simple phase-field model for interface tracking in three dimensions, Comput. Math. Appl. 78 (4) (2016) 1154–1165.

[17] M.H.M. Sulman, Optimal mass transport-based adaptive mesh method for phase-field models of two-phase fluid flows, Comput. Math. Appl. 72 (9) (2016) 2181–2193.

[18] H. Liang, B. Shi, Z. Chai, An efficient phase-field-based multiple-relaxation-time lattice Boltzmann model for three-dimensional multiphase flows, Comput. Math. Appl. 73 (7) (2017) 1524–1538.

[19] Y. Li, Q. Xia, S. Yoon, C. Lee, B. Lu, J. Kim, A simple and efficient volume merging method for triply periodic minimal structure, Comput. Phys. Comm. 264 (2021) 107956.

[20] Y. Li, Q. Yu, W. Fang, B. Xia, J. Kim, An unconditional stable second-order BDF scheme for the three-dimensional Cahn–Hilliard–Hele–Shaw system, Adv. Comput. Math. 47 (3) (2021).

[21] Q. Xia, Q. Yu, Y. Li, A second-order accuracy, unconditionally energy stable numerical scheme for binary fluid flows on arbitrarily curved surfaces, Comput. Methods Appl. Mech. Engrg. 384 (1) (2021) 113987.

[22] J.W. Cahn, J.E. Hilliard, Free energy of a nonuniform system. I: Interfacial free energy, J. Chem. Phys. 28 (2) (1958) 258–267.

[23] L. Leibler, Theory of microphase separation in block copolymers, Macromolecules 13 (6) (1980) 1602–1617.

[24] T. Ohta, K. Kawasaki, Equilibrium morphology of block copolymer melts, Macromolecules 19 (10) (1986) 2621–2632.

[25] T. Ohta, K. Kawasaki, Comment on the free energy functional of block copolymer melts in the strong segregation limit, Macromolecules 23 (8) (1990) 2413–2414.

[26] T. Ohta, A. Ito, Dynamics of phase separation in copolymer/homopolymer mixtures, Phys. Rev. E 52 (5) (1995) 5250–5260.

[27] T. Uneyama, M. Doi, Density functional theory for block copolymer melts and blends, Macromolecules 38 (1) (2005) 196–205.

[28] T. Uneyama, Density functional simulation of spontaneous formation of vesicle in block copolymer solutions, J. Chem. Phys. 126 (11) (2007).

[29] H.H. Gidey, B.D. Reddy, Operator-splitting methods for the 2D convective Cahn–Hilliard equation, Comput. Math. Appl. 77 (12) (2019) 3128–3153.

[30] T. Aboelenen, H.M. El-Hawary, A high-order nodal discontinuous Galerkin method for a linearized fractional Cahn–Hilliard equation, Comput. Math. Appl. 73 (6) (2016) 1197–1217.

[31] S.M. Choo, S.K. Chung, K.I. Kim, Conservative nonlinear difference scheme for the Cahn–Hilliard equation, Comput. Math. Appl. 36 (7) (1998) 31–39.

[32] Y. Li, J.-I. Choi, J. Kim, Multi-component Cahn–Hilliard system with different boundary conditions in complex domains, J. Comput. Phys. 323 (2016) 1–16.

[33] Y. Li, H.-G. Lee, B. Xia, J. Kim, A compact fourth-order finite difference scheme for the three-dimensional Cahn–Hilliard equation, Comput. Phys. Comm. 200 (2016) 108–116.

[34] Y. Li, J. Kim, Nan Wang, An unconditionally energy-stable second-order time-accurate scheme for the Cahn–Hilliard equation on surfaces, Commun. Nonlinear Sci. Numer. Simul. 53 (2017) 213–227.

[35] Y. Li, Y. Choi, J. Kim, Computationally efficient adaptive timestep method for the Cahn–Hilliard equation, Comput. Math. Appl. 73 (8) (2017) 1855–1864.

[36] X. Wu, Y.A. Dzenis, Phase-field modeling of the formation of lamellar nanostructures in diblock copolymer thin films under inplanar electric fields, Phys. Rev. E 77 (3) (2008) 1–10.

[37] K.B. Glasner, Multilayered equilibria in a density functional model of copolymer-solvent mixtures, SIAM J. Math. Anal. 49 (2) (2017) 1593–1620.

[38] K.B. Glasner, S. Orizaga, Multidimensional equilibria and their stability in copolymer-solvent mixtures, Physica D 375 (15) (2018) 1–12.

[39] Q. Cheng, X. Yang, J. Shen, Efficient and accurate numerical schemes for a hydro–dynamically coupled phase field diblock copolymer model, J. Comput. Phys. 341 (15) (2017) 44–60.

[40] J. Zhao, X. Yang, Y. Gong, X. Zhao, X. Yang, J. Li, Q. Wang, A general strategy for numerical approximations of non-equilibrium models–part I: thermodynamical systems, Int. J. Numer. Anal. Model. 15 (6) (2018) 884–918.

[41] J. Zhao, H. Li, Q. Wang, X. Yang, A linearly decoupled energy stable scheme for phase field models of three-phase incompressible viscous fluid flows, J. Sci. Comput. 70 (2017) 1367–1389.

[42] Y. Gong, J. Zhao, Q. Wang, Arbitrarily high-order linear unconditionally energy stable schemes for gradient flow models, J. Comput. Phys. 419 (15) (2020) 109610.

[43] Y. Gong, J. Zhao, Q. Wang, Arbitrarily high-order unconditionally energy stable schemes for thermodynamically consistent gradient flow models, SIAM J. Sci. Comput. 42 (1) (2020) B135–B156.

[44] Y. Gong, J. Zhao, Q. Wang, Linear second-order energy stable schemes for hydrodynamic models of binary mixtures based on a spatially pseudospectral approximation, Adv. Comput. Math. 44 (5) (2018) 1573–1600.

[45] E. Avalos, T. Teramoto, H. Komiyama, H. Yabu, Y. Nishiura, Transformation of block copolymer nanoparticles from ellipsoids with striped lamellae into onionlike spheres and dynamical control via coupled Cahn–Hilliard equations, ACS Omega 3 (1) (2018) 1304–1314.

[46] Y. Han, Z. Xu, A. Shi, L. Zhang, Pathways connecting two opposed bilayers with a fusion pore: a molecularly-informed phase field approach, Soft Matter 16 (2) (2020) 366–374.

[47] H. Garcke, B. Nestler, B. Stoth, A multiphase field concept: Numerical simulations of moving phase boundaries and multiple junctions, SIAM J. Appl. Math. 60 (1) (1999) 295–315.

[48] E. Avalos, T. Higuchi, T. Teramoto, H. Yabu, Y. Nishiura, Frustrated phases under three-dimensional confinement simulated by a set of coupled Cahn–Hilliard equations, Soft Matter 12 (27) (2016) 5905–5914.

[49] R. Choksi, M.A. Peletier, J.F. Williams, On the phase diagram for microphase separation of diblock copolymers: An approach via a nonlocal Cahn–Hilliard functional, SIAM J. Appl. Math. 69 (6) (2009) 1712–1738.

[50] R. Choksi, Scaling laws in microphase separation of diblock copolymers, J. Nonlinear Sci. 11 (3) (2001) 223–236.

[51] T. Ohta, M. Nonomura, Elastic property of bilayer membrane in copolymer–homopolymer mixtures, Eur. Phys. J. B 2 (1) (1998) 57–68.